RSC Advances

PAPER

View Article Online
View Journal | View Issue

Cite this: *RSC Adv.*, 2017, **7**, 45834

Hydrothermal synthesis of narrow-band red emitting $K_2NaAlF_6:Mn^{4+}$ phosphor for warm-white LED applications

Haiming Cheng, Yan Song, Guixia Liu,* Dan Li, Xiangting Dong, Jinxian Wang and Wensheng Yu

A series of Mn^{4+} activated aluminofluoride (K_2NaAlF_6) red phosphors were synthesized *via* a hydrothermal route. The structure, morphology and composition were characterized by X-ray diffraction (XRD), scanning electron microscopy (SEM) and energy-dispersive X-ray spectrometry (EDX). The photoluminescence properties were investigated by using emission and excitation spectra, temperature dependent luminescence spectra and decay curves. The obtained $K_2NaAlF_6:Mn^{4+}$ can emit red light peaking at 633 nm under 460 nm excitation. The critical quenching concentration of Mn^{4+} was about 1%. The changes in Mn^{4+} emissions based on different ratios of KF to NaF, reaction temperature and reaction time were investigated in detail. Concentration and thermal quenching mechanisms were elucidated systematically. The white light-emitting diodes (WLED) fabricated with the as-prepared phosphor exhibit a low color temperature (4310 K), higher color rendering index (R_a = 78.7) and luminous efficacy of 60.22 lm W^{-1}. The inherent advantage of $K_2NaAlF_6:Mn^{4+}$ makes it a promising red phosphor for future WLED.

Received 31st August 2017
Accepted 20th September 2017

DOI: 10.1039/c7ra09671b

rsc.li/rsc-advances

1 Introduction

In recent years, white light-emitting diodes (WLED), which are considered as energy-saving light source, have attracted more and more attention owing to their long operational life time, environmentally friendly properties and stability.[1–5] Currently, the white light is mainly produced *via* a combination of leaked blue emission from an InGaN chip and the broad green-yellow emission of yellow phosphor $Y_3Al_5O_{12}:Ce^{3+}$ ($YAG:Ce^{3+}$).[6–8] However, this approach limits the application range to cool white light with poor color rendering and a correlated higher colour temperature of approximately 4500–8000 K.[9,10] The innate deficiency in the red spectral region reduces the suitability for indoor illumination. It is therefore logical to supplement a red phosphor into this system to improve the color rendering. This idea has stimulated research on red phosphors activated by rare earth or transition metal ions.

Among the available red phosphors, Eu^{2+} or Ce^{3+} ions doped nitrides are the most widely known, such as $Sr_2Si_5N_{18}:Eu^{2+}$, $CaAlSiN_3:Eu^{2+}$ and $M_2Si_5N_8:Ce^{3+}$ (M = Ca, Sr, Ba).[11–13] Eu^{2+} doped nitrides and oxides have the advantages of high quantum efficiency and good thermal stability. However, the preparation process and reaction conditions of nitrides phosphors are rigorous.[14–16] These shortcomings limit the application in white LEDs. Compared with the rare earth ions doped nitrides red phosphor, tetravalent manganese ions (Mn^{4+}) doped fluoride or oxide phosphors exhibit a series of obvious advantages.[17,18] First of all, Mn^{4+} ions display the characteristics of narrow emission and high color purity, which overcome the defect of broad emission bands and serious photon reabsorption in Eu^{2+} doped nitrides phosphors.[19] In addition, the low price of transition metals effectively reduces the producing cost of LEDs. It is another important advantage that the Mn^{4+} ions activated phosphors can be excited by blue light chip. At present, Mn^{4+} doped oxide phosphors have attracted much attention.[20–22] The Jin's team reported a class of Mn^{4+} doped $SrGe_4O_9$ red phosphors by conventional solid-state reaction.[23] The Mn^{4+} can replace Ge^{4+} sites in the host lattice owing to the same ionic radius of Mn^{4+} and Ge^{4+}. $SrGe_4O_9:Mn^{4+}$ phosphors exhibit red emission under excitation of 276 nm and 430 nm. In general, the near ultraviolet absorption peaks of Mn^{4+} doped oxide phosphors are higher than those of blue light, this property also limits the use of blue light chip. Therefore, numerous researchers have devoted their effort to investigate Mn^{4+}-substituted fluoride phosphor containing AF_6^{2-} (A = Ti^{4+}, Ge^{4+}, Si^{4+}, Sn^{4+}, Zr^{4+}) octahedral environment.[24,25] The outer $3d^3$ electron configurated Mn^{4+} activated phosphor shows two intense broad absorption bands ranged from 300 to 500 nm, attributing to spin-allowed $^4A_{2g} \rightarrow {}^4T_{1g}$ and $^4A_{2g} \rightarrow {}^4T_{2g}$ transition.[26,27] The red emission near 600–700 nm under blue light excitation originates from the spin-forbidden $^2E_g \rightarrow {}^4A_{2g}$

Key Laboratory of Applied Chemistry and Nanotechnology at Universities of Jilin Province, Changchun University of Science and Technology, Changchun, China. E-mail: liuguixia22@163.com; Fax: +86-431-85383815; Tel: +86-431-85582574

transition.[28] For example, Zhou and his co-authors synthesized an efficient red phosphor $BaGeF_6:Mn^{4+}$ by hydrothermal method and obtained the optimized reaction conditions.[29] In addition, $BaGeF_6:Mn^{4+}$ is favourable for decreasing correlated color temperature (CCT) in WLED devices. Nguyen's group reported a co-precipitation method to produce a class of $Na_2SiF_6:Mn^{4+}$ red phosphor using $NaOH/NaMnO_4$ as starting materials in SiF_6^{2-}/HF system.[30] The result displayed the relative luminescence intensity maintained to 92% at 423 K than that at room temperature. Recently, Zhu's group[31] had successfully prepared novel red-emitting phosphors $K_2LiGaF_6:Mn^{4+}$ with excellent thermal stability and luminescent properties, it was proved to be a potential commercial phosphor used in warm white LED devices. Huang's group[32] had synthesized Mn^{4+} doped K_2SiF_6 phosphors using a novel HF-free hydrothermal synthetic. The synthetic route was more environmental friendly and the reaction mechanism of $K_2SiF_6:Mn^{4+}$ was discussed in detail. According to the previous studies, it is not difficult to find that Mn^{4+} doped oxide or fluoride phosphors can exhibit red emission and effectively improve the performance of LEDs. K_2NaAlF_6 is a common elpasolite material. The crystal structure of K_2NaAlF_6 shows that Al^{3+} is surrounded by six F^- ions. The AlF_6^{3-} octahedron environment is beneficial for the emission of Mn^{4+}.[33] Furthermore, the ionic radius of Al^{3+} and Mn^{4+} are similar. Mn^{4+} ions may be achieved by replacing Al^{3+} after entering the crystal lattice. Thus, we believe that K_2NaAlF_6 can be used as a suitable matrix for luminescent materials.

In this paper, we report a kind of elpasolite structure red phosphor $K_2NaAlF_6:Mn^{4+}$. The crystal structure and luminescence properties are investigated. Al^{3+} ions can be substituted by Mn^{4+} ions because of the smaller ionic radius. Meanwhile, the influences of synthesis conditions, such as raw material, reaction time, temperature and Mn^{4+} concentration on emission intensity have been discussed carefully in details. The experiment results show that $K_2NaAlF_6:Mn^{4+}$ phosphor is a promising red phosphor for future WLED.

2 Experimental

2.1 Materials

All the chemical reagents in our experiment, including potassium fluoride (KF, >98%), sodium fluoride (NaF, >98%), aluminium fluoride (AlF_3, >99%), hydrofluoric acid solution (HF, 40 wt%), potassium permanganate ($KMnO_4$, >99.5%), potassium hydrogen difluoride (KHF_2, >99%) and hydrogen peroxide aqueous solution (H_2O_2, 30.0%), were supplied by the Sinopharm Chemical Reagent Co. Ltd. All chemical reagents were used as obtained without further purification.

2.2 Preparation

Red phosphor $K_2NaAlF_6:Mn^{4+}$ was prepared *via* a hydrothermal route with K_2MnF_6 as the Mn^{4+} source. The K_2MnF_6 crystals were prepared based on Bode's method.[34] In a typical synthesis, AlF_3 (0.2444 g) and K_2MnF_6 (0.0222 g) were added to the 20 mL 40 wt% HF solution in a 50 mL plastic breaker. The mixture was fully dissolved by magnetically stirring. Subsequently, NaF (0.1260 g) and KF (0.3487 g) were added into 20 mL distilled water until completely dissolved. Finally, a mixture of the NaF and KF was put into the above solution. After vigorous stirring for 30 min, the mixture solution was transferred into a 50 mL Teflon-lined autoclave and heated at 180 °C for 6 h, then cooled naturally to room temperature. The yellow solid products were collected by centrifugation, washed several times with distilled water and ethanol. The as-prepared products were dried for 12 h at 60 °C. Finally, the $K_2NaAlF_6:Mn^{4+}$ red phosphor sample was obtained. The synthesis diagram of the preparation process is revealed in Fig. 1.

2.3 Fabrication of LED devices

The WLED devices were fabricated by combining GaN chips (~460 nm) with the mixture of obtained red phosphors $K_2NaAlF_6:Mn^{4+}$ and yellow phosphor $YAG:Ce^{3+}$. First, the phosphors were completely mixed with epoxy resin, and then the mixture was coated onto the superficies of the GaN chip. The device was packaged with epoxy resin and solidified at 140 °C for 12 h. The fabricated devices were used for subsequent testing.

2.4 Characterizations

The crystal structures of all samples were investigated using a RigakuD/max-RA X-ray diffractometer with Cu Kα radiation (λ = 0.15418 nm) in the 2θ range from 10° to 90°. The corresponding surface morphology and composition of the samples were examined by a FEI XL-30 field emission scanning electron microscope (FESEM) equipped with an attached energy dispersive X-ray (EDX) spectrometer. Photo-luminescence (PL), photoluminescence excitation (PLE) and luminescence decay curves of samples were measured on a HITACHI F-7000 fluorescence spectrophotometer equipped with a 150 W Xe lamp as the excitation source, scanning at 1200 nm min^{-1}. The temperature dependent luminescence properties were examined using a JobinYvon fluoro Max-4 equipped with a 150 W xenon lamp as the excitation source. Quantum efficiency was also measured using a photoluminescence quantum efficiency measurement system (C9920-02, Hamamatsu Photonics K. K., Japan).

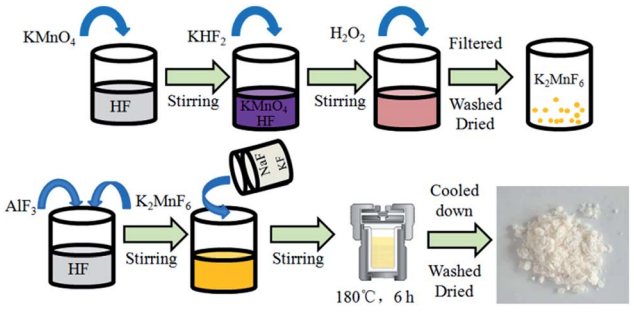

Fig. 1 Synthesis diagram of $K_2NaAlF_6:Mn^{4+}$ phosphors *via* a hydrothermal method.

3 Results and discussion

3.1 Phase structure and morphology analysis

The phase purity and crystallinity of the as-prepared K_2NaAlF_6:Mn^{4+} samples were first characterized by XRD. Fig. 2(a) shows the XRD pattern of the K_2NaAlF_6:Mn^{4+} sample along with JCPDS card no. 22-1235 at the bottom. The diffraction peaks of the phosphors can be matched well with the standard pattern of pure K_2NaAlF_6. No extra peaks of impurity are detected in the pattern, indicating the doped Mn^{4+} ions do not change the crystal structure of K_2NaAlF_6. The K_2NaAlF_6 is crystallized in a cubic $Fm\bar{3}m$ space group with lattice parameter of $a = b = c =$ 8.122 Å. Fig. 2(b) displays the crystal structure of the K_2NaAlF_6. Al^{3+} is coordinated with six F^- to form a regular AlF_6^{3-} octahedron. Mn^{4+} ions would prefer to replace Al^{3+} ions in octahedral sites. Because Mn^{4+} (0.53 Å, CN = 6) has highly close ionic radius with Al^{3+} (0.535 Å, CN = 6).

The morphology and composition of the as-prepared K_2NaAlF_6:Mn^{4+} were characterized by FESEM and EDX analysis, respectively. As show in Fig. 3(a), it can be seen that the as-prepared phosphor displays truncated octahedron morphology with smooth surface. A side length of truncated octahedron is about 1 μm. In the corresponding EDX spectrum (Fig. 3(b)), the results exhibit that the phosphors are composed of K, Na, Al, F and Mn element, respectively. The result also verifies that Mn element has been indeed doped into the lattice to occupy the Al lattice site. The detected C and Au element in Fig. 3(b) is ascribed to the conducting resin and metal spraying. The peak of the Si results from the silicon wafer used during the measurement.

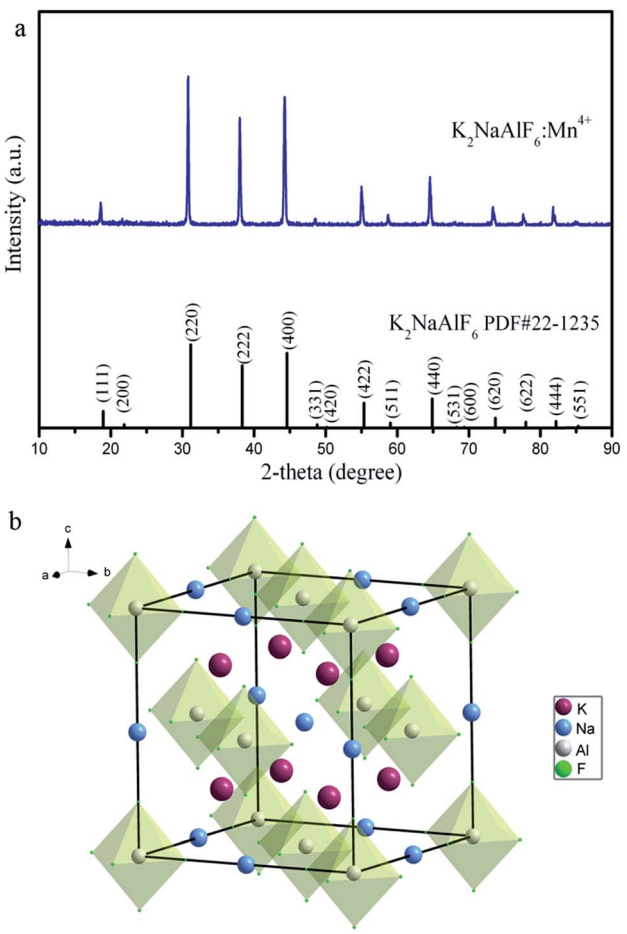

Fig. 2 (a) XRD pattern of the as-synthesized K_2NaAlF_6:Mn^{4+} samples. The standard card (PDF#22-1235) is included for reference. (b) Schematic illustration of K_2NaAlF_6 crystal structure.

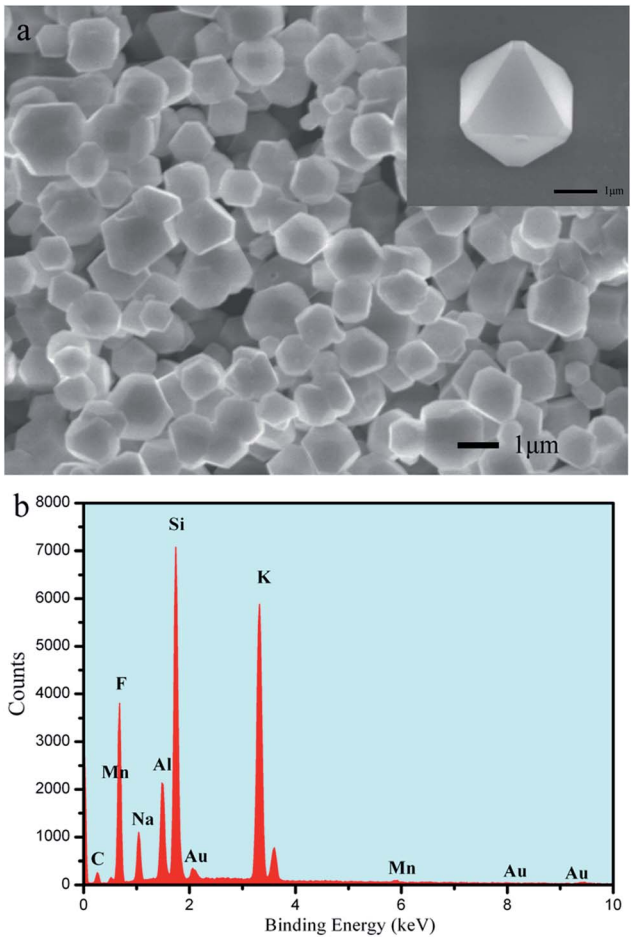

Fig. 3 (a) SEM images (a) and EDX spectrum (b) of K_2NaAlF_6:3%Mn^{4+}.

3.2 Luminescence properties of K_2NaAlF_6:Mn^{4+}

To determine the luminescence behaviour of Mn^{4+} in K_2NaAlF_6, we choose the samples by hydrothermal treatment at 180 °C for 6 h as an example. Fig. 4(a) presents the typical excitation and emission spectra at room temperature. As the monitoring wavelength at 633 nm, the photoluminescence excitation spectrum of K_2NaAlF_6:Mn^{4+} could be recorded in the wavelength range of 300–550 nm. There are two excitation bands located in the near-UV and blue region. The shape and range of excitation spectrum are basically consistent with those reported in the literature.[35] The weak excitation peak at 363 nm can be ascribed to the spin-allowed $^4A_{2g} \rightarrow {}^4T_{1g}$ transition of Mn^{4+} ions in K_2NaAlF_6. The dominating excitation peak at 460 nm is due to the transition from ground state $^4A_{2g}$ to $^4T_{2g}$ of Mn^{4+} ions.

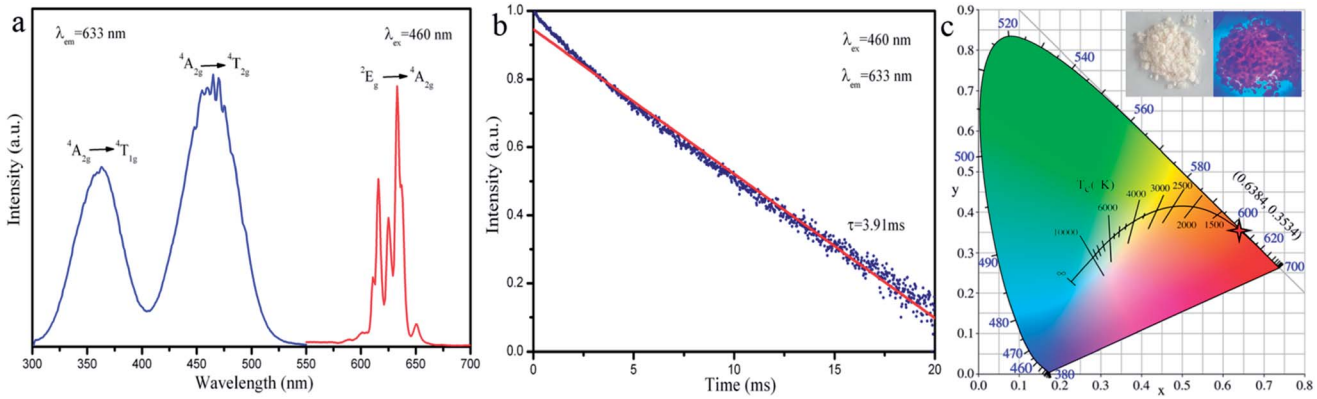

Fig. 4 (a) Photoluminescence excitation (left) and emission (right) spectra, (b) decay curve of the K_2NaAlF_6:3%Mn^{4+} examined at room temperature by monitoring wavelength at 633 nm with a 460 nm light excitation and (c) CIE chromaticity coordinate of K_2NaAlF_6:3%Mn^{4+}. The inset photographs represent the K_2NaAlF_6:3%Mn^{4+} phosphor in the daylight and under lamp (460 nm) irradiation.

The results demonstrate the excitation of K_2NaAlF_6:Mn^{4+} can be well matched with the GaN blue chip and the prepared phosphors have a potential application for LEDs. Under excitation at 460 nm, the emission spectrum has series of narrow-line emission peaks ranged from 580 to 660 nm, with the maximum peak at 633 nm. The red emission line is attributed to $^2E_g \rightarrow {}^4A_{2g}$ transition of Mn^{4+}. The fluorescence decay curve for $^2E_g \rightarrow {}^4A_{2g}$ of the Mn^{4+} ions in red phosphor K_2NaAlF_6:3%Mn^{4+} monitored at 633 nm with the excitation of 460 nm was measured at room temperature, as shown in Fig. 4(b). The decay curve can be well fitted to a single-exponential model by the following equation:

$$I_{(t)} = I_0 + Ae^{(-t/\tau)}$$

where $I_{(t)}$ is the luminescence intensity of K_2NaAlF_6:3%Mn^{4+} at time t, A is constant, I_0 is the initial intensity and τ is the lifetime for exponential components. The fluorescence lifetime value is about 3.91 ms. Fig. 4(c) displays the CIE chromaticity diagram of K_2NaAlF_6:3%Mn^{4+}. The K_2NaAlF_6:Mn^{4+} red phosphor has aquantum efficiency of 16%. The CIE chromaticity coordinates of as-prepared phosphor were calculated to be $x = 0.6384$, $y = 0.3534$, which is very close to the standard values of National Television Standard Committee (NTSC) ($x = 0.67$, $y = 0.33$). Therefore, K_2NaAlF_6:3%Mn^{4+} can exhibit a high red purity. The inset photographs in Fig. 4(c) represent the K_2NaAlF_6:3%Mn^{4+} phosphor in the daylight and blue light illumination, respectively. One can see obvious red emission light under blue light radiation.

The ratio of reactants is an important parameter for the phase purity and luminous intensity. In order to acquire better luminescent properties of the phosphors, we investigated the influence of different molar ratio of KF to NaF on crystal structure and luminescence properties. Fig. 5(a) shows the XRD patterns of K_2NaAlF_6:Mn^{4+} phosphors synthesized with different molar ratio of KF to NaF (1 : 1, 2 : 1, 4 : 1, 8 : 1, 12 : 1 and 20 : 1). When the molar ratio of KF to NaF is 1 : 1, the major diffraction peaks are close to the standard card PDF#22-1235. The three main diffraction peaks correspond to the lattice plane [220], [222] and [400], respectively, and the diffraction intensity is very close. However, a weak impurity peak also appears near the diffraction angle about 30.6°, which is accordance with the standard card no. 30-1144 ($Na_5Al_3F_{14}$). The result

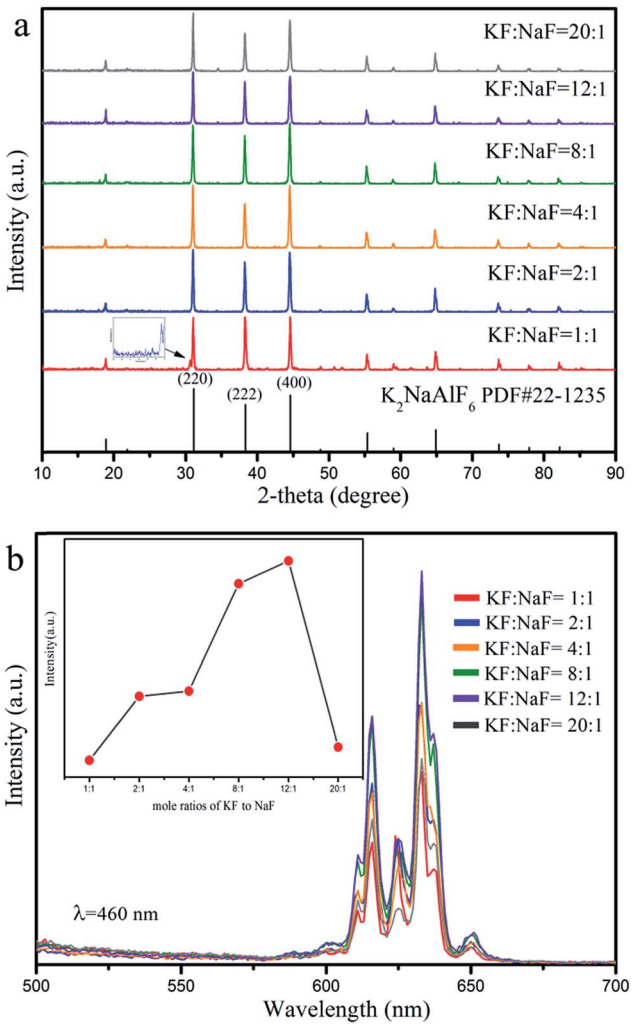

Fig. 5 (a) XRD patterns and (b) emission spectra ($\lambda_{ex} = 460$ nm) of the K_2NaAlF_6:Mn^{4+} phosphors synthesized with different molar ratios of KF to NaF (KF : NaF = 1 : 1, 2 : 1, 4 : 1, 8 : 1, 12 : 1 and 20 : 1).

implies that a part of impurity $Na_5Al_3F_{14}$ can be generated in case of insufficient potassium source. When the molar ratio of KF to NaF gradually rises to 2 : 1–20 : 1, all the diffraction peaks of as-prepared samples can be in agreement with the JCPDS card no. 22-1235. No other impurity phases, such as $Na_5Al_3F_{14}$ or Na_3AlF_6 are detected, indicating that the product is pure phase. Fig. 5(b) is the emission spectra of K_2NaAlF_6:Mn^{4+} prepared with different molar ratio of KF to NaF. It can be seen that all the PL spectra of K_2NaAlF_6:3%Mn^{4+} are almost identical except for the luminescence intensity. When molar ratio of KF to NaF is 1 : 1, the red emission intensity is weak. With increasing the mole ratio of KF to NaF from 2 : 1 to 12 : 1, the red emission can be enhanced, the red emission intensity of sample (KF : NaF = 12 : 1) is about 1.52 times higher than that of samples (KF : NaF = 2 : 1), suggesting that appropriate adding the ratio of KF to NaF into the reaction system may enhance the intensity of Mn^{4+} doped K_2NaAlF_6 phosphor. But further increasing the ratio of KF to NaF, a weakening trend of emission spectrum is observed, which might be due to excessive K^+ exacerbated the charge imbalance when the tetravalent Mn^{4+} replaced the trivalent Al^{3+}.

In order to investigate the effect of the reaction temperature on the phase and photoluminescence properties of K_2NaAlF_6:Mn^{4+} phosphors. A series of K_2NaAlF_6:Mn^{4+} samples were synthesized at different temperatures for 6 h. Fig. 6(a) presents the XRD patterns of the phosphors obtained at different reaction temperatures. It is obviously seen that the diffraction peaks of these phosphors agree well with the cubic phase K_2NaAlF_6 [space group: $Fm\bar{3}m$] (PDF#22-1235), without any impurity phase. The increasing of the reaction temperature did not cause the change of the crystal structure and phase purity. Fig. 6(b) displays a series of corresponding emission spectra of K_2NaAlF_6:Mn^{4+} prepared under the reaction temperatures from 25 °C to 180 °C. Noted that the emission spectra also share the similar shape. With increasing the reaction temperature from 25 °C to 100 °C, the emission intensity sharply increases. Improving the proper reaction temperature can be beneficial for Mn^{4+} into the lattice to substitute Al^{3+} sites. Further increasing reaction temperature, the luminescent intensity of the as-synthesized K_2NaAlF_6:Mn^{4+} phosphor decreases obviously under 460 nm blue light excitation. The possible reason is that the Mn^{4+} is not stable at very high temperature.

In addition to the molar ratio of raw materials and reaction temperature, the influence of reaction time on the luminescence of K_2NaAlF_6:Mn^{4+} was also discussed. Fig. 7(a) presents the XRD patterns of the products obtained by different hydrothermal reaction times. It demonstrates that all the diffraction peaks are consisted with the standard data (PDF#22-1235) of K_2NaAlF_6 with a cubic structure. The phase purity and crystal structure of samples exhibit no significant change with increasing reaction times. The emission spectra of K_2NaAlF_6:Mn^{4+} prepared at different reaction times are shown in Fig. 7(b). The K_2NaAlF_6:Mn^{4+} phosphors all display sharp red emission peaks covering from 550 nm to 700 nm with a maximum at 633 nm. It is clear that the emission intensity of as-prepared sample at 12 h is stronger than that of 6 h. As the reaction time further increases, the emission intensity of the

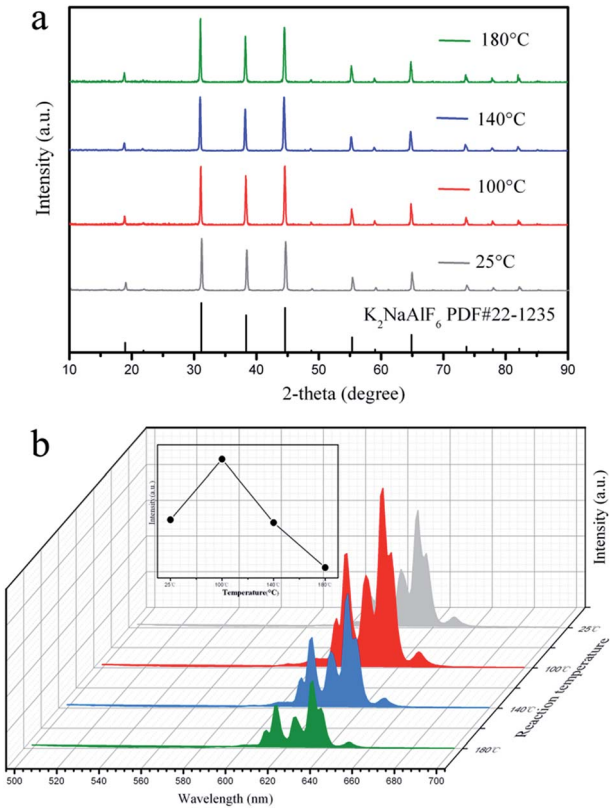

Fig. 6 (a) XRD patterns and (b) emission spectra (λ_{ex} = 460 nm) of the K_2NaAlF_6:Mn^{4+} samples synthesized at different reaction temperatures.

K_2NaAlF_6:Mn^{4+} decreases. The phenomenon of emission intensity dropped with prolonging reaction time from 12 h to 36 h may be due to the Mn^{4+} ions in the phosphors tend to instability in a long period time.[36] Therefore, fluorescence quenching results in lower luminous intensity.

The next part mainly concerns the influence of optical properties and structure for K_2NaAlF_6:Mn^{4+} prepared using various Mn^{4+} ions contents. As shown in Fig. 8(a), the XRD patterns of the obtained K_2NaAlF_6:xMn^{4+} (x = 0.5%, 1%, 3%, 5% and 7%) phosphors are collected to verify the phase purity. All the characteristic diffraction peaks are in good agreement with the corresponding standard card data of K_2NaAlF_6 (PDF#22-1235). The results show that the Mn^{4+} ions enter the lattice of K_2NaAlF_6 without altering the crystal structure. The high diffraction intensities indicate that the phosphors have good crystallinity. Fig. 8(b) shows the emission spectra of K_2NaAlF_6:Mn^{4+} with different Mn^{4+} doping concentrations. A series of emission peaks located at 611, 616, 625, 633 and 650 nm can be observed from the corresponding emission spectra of K_2NaAlF_6:Mn^{4+} under 460 nm blue light excitation. With increasing the concentration of Mn^{4+} ions, the emission intensity of as-prepared phosphor increases. When the manganese content reaches 1%, the sample obtains the strongest emission intensity. When further increasing Mn^{4+} ions concentration beyond 1%, the emission intensities of K_2NaAlF_6:Mn^{4+} have an obvious decreasing trend, which might be related to concentration quenching effect. Therefore, the

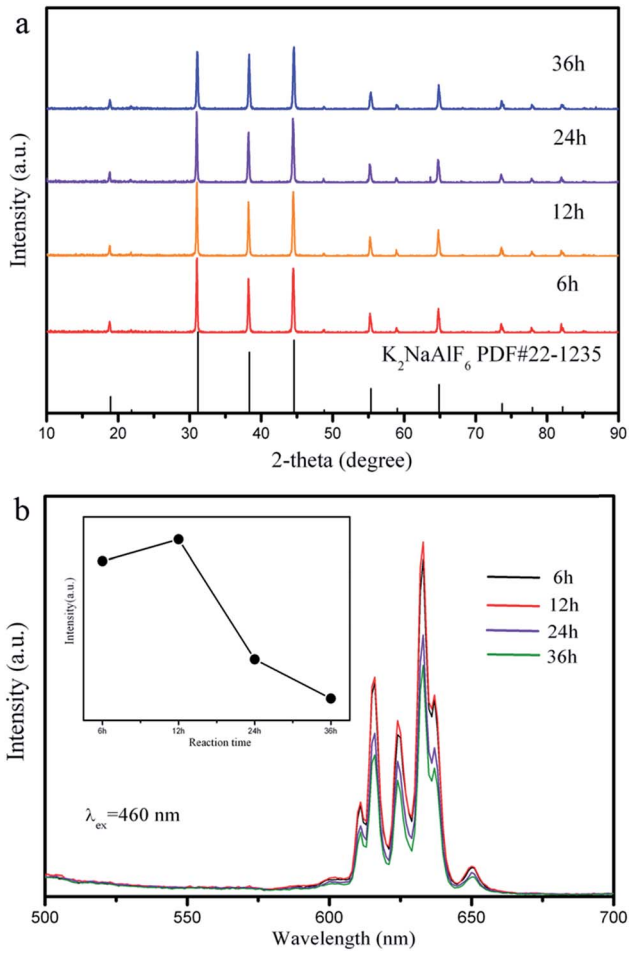

Fig. 7 (a) XRD patterns and (b) emission spectra (λ_{ex} = 460 nm) of the K_2NaAlF_6:Mn^{4+} samples synthesized at different reaction times.

optimum Mn^{4+} ions concentration in K_2NaAlF_6 host should be 1%, indicating that 1% is the quenching concentration in K_2NaAlF_6:Mn^{4+} phosphor. The phenomenon of the dropped emission intensity can be attributed to the occurrence of energy transfer within the adjacent Mn^{4+}, which is finally end by a kill centre. Evidently, the energy transfer mechanism is not caused by radiation re-absorption. Because there is no overlap between PLE and PL spectra of K_2NaAlF_6:xMn^{4+}. The exchange interaction or the dipole–dipole interaction may be responsible for the quenching. To clarify the point, the critical distance (R_c) was calculated with the following equation:[37]

$$R_c \approx 2 \times \left(\frac{3V}{4\pi x_c N}\right)^{\frac{1}{3}}$$

where V is the volume of unit cell, x_c means the critical concentration. N is the number of the central cations in the unit cell. For K_2NaAlF_6:Mn^{4+}, V = 534.99 Å, x_c = 0.01 and N = 4. Therefore, the critical distance of R_c is calculated to be 14.735 Å, which is larger than the typical critical distance (5 Å), so the possibility of exchange interaction is eliminated. The concentration quenching is related to multipolar energy transfer mechanism. According to the Dexter theory, the type of interaction between Mn^{4+} ions can be determined by the equation[38] as follows:

$$\frac{I}{x} = K\left[1 + \beta(x)\frac{\theta}{3}\right]^{-1}$$

where I is the emission intensity at activator concentration x, K and β are constants, the value of θ = 6, 8, 10 represents the electric multipole index corresponding to the dipole–dipole (d–d), dipole–quadrupole (d–q) and quadrupole–quadrupole (q–q) interaction. The above equation can be predigested to

$$\log\left(\frac{I}{x}\right) = -\frac{\theta}{3}\log x + A$$

Fig. 8(c) shows the dependence of $\log(I/x)$ on $\log(x)$ with a slope of $(-\theta/3)$. A relative linear fitted can be obtained and the result of the slope is about 1.3. The value of θ is calculated approximately 6. Therefore, the mechanism of the concentration quenching of Mn^{4+} is d–d interaction in K_2NaAlF_6 host.

3.3 Temperature stability properties

The thermal stability of the phosphors is frequently used as an important parameter in LED applications. In order to investigate the influence of temperature on the luminescence of

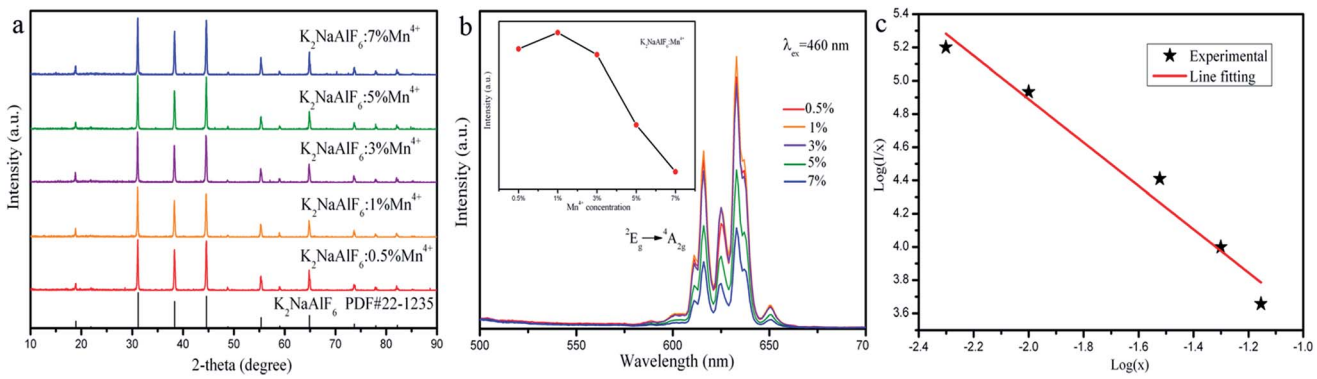

Fig. 8 (a) XRD patterns, (b) emission spectra (λ_{ex} = 460 nm) of the as-synthesized K_2NaAlF_6:xMn^{4+} (x = 0.5%, 1%, 3%, 5% and 7%), the inset photograph represents emission intensity of Mn^{4+} as a function of Mn^{4+} doping concentration, and (c) the relation plot of $\log(I/x)$ on $\log(x)$ of Mn^{4+} doping concentration x.

$K_2NaAlF_6:Mn^{4+}$ phosphor, a series of emission spectra for $K_2NaAlF_6:Mn^{4+}$ in the temperature range of 98–498 K was shown in Fig. 9(a). All the emission peaks are in same shape. As an increase of temperature, the positions of the emission peak have no obvious shift with the strongest emission peak at ~633 nm. The luminous intensity displays a decreasing trend with an increase in temperature from 98 K to 498 K. Fig. 9(b) displays the relative intensity trend at 633 nm of $K_2NaAlF_6:Mn^{4+}$. Increasing the temperature, the luminous intensity decreases gradually. Upon heating the phosphor to 448 K, the emission intensity remains approximately 65% of the emission intensity at 298 K. The phenomenon of thermal quenching is attributed to the non-radiative transition, which can be fitted by the following equation:[39]

$$I_T = \frac{I_0}{1 + c \times \exp\left(-\frac{\Delta E}{kT}\right)}$$

where I_T is the intensity at temperature T, I_0 is the initial intensity, c is the frequency factor, ΔE is the activation energy of the thermal quenching and K is the Boltzmann constant (8.629×10^{-5} eV K^{-1}). According to the above equation, the activation energy of the as-prepared $K_2NaAlF_6:Mn^{4+}$ red phosphor is 0.3 eV, suggesting the excellent thermal stability. The phenomenon of thermal quenching can be illustrated by configuration coordinate diagram (Fig. 9(c)). Under near UV and blue light excitation, the electrons are excited to the excited state, from $^4A_{2g}$ to $^4T_{1g}$ and $^4T_{2g}$ levels of Mn^{4+} ions in K_2NaAlF_6 hosts. Subsequently, the electrons of ^2E_g level transit to the ground state $^4A_{2g}$ level by radiative transition, which brings out the red emission of Mn^{4+} ions. As the temperature increases, a part of the electrons absorbing activation energy ΔE go back to the ground state *via* the crossover point of the states of $^4T_{2g}$ and $^4A_{2g}$, resulting in non-radiation transition to ground state $^4A_{2g}$ and the formation of thermal quenching.

3.4 Luminescence performance of WLEDs

To validate the availability of $K_2NaAlF_6:Mn^{4+}$ for the blue-based white LED application, the synthesized red phosphor $K_2NaAlF_6:Mn^{4+}$ was mixed with the YAG:Ce^{3+} and the mixture coupled with a 460 nm blue LED to fabricate a WLED. Fig. 10(a) displays the electroluminescence spectra of the blue light chip, LED composed of blue light chip and YAG:Ce^{3+}, YAG:Ce^{3+}–

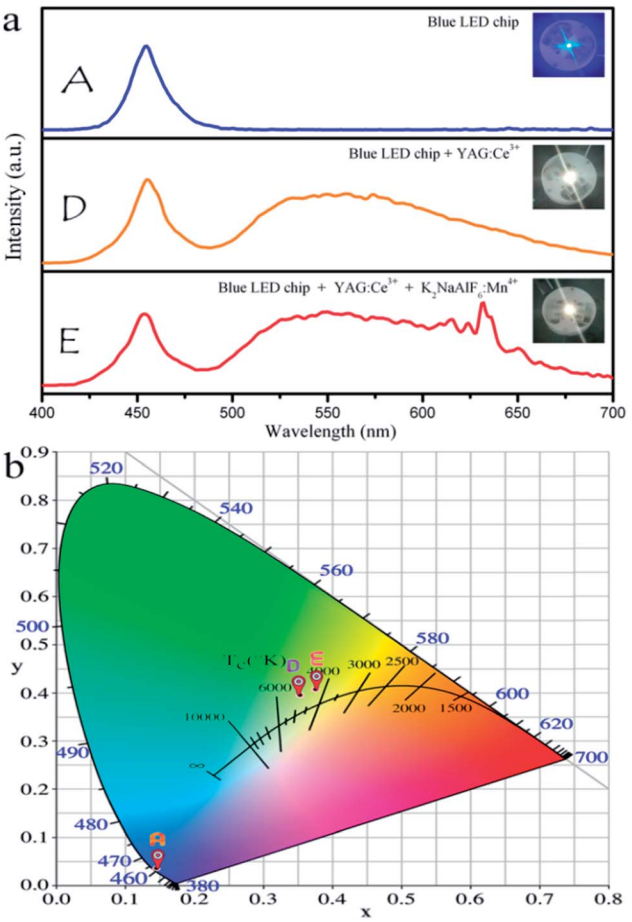

Fig. 10 (a) Electroluminescence spectra of blue chip, LED assembling the blue light chip – YAG:Ce^{3+}, and YAG:Ce^{3+}–$K_2NaAlF_6:Mn^{4+}$ under 20 mA current excitation. (b) The corresponding CIE chromaticity coordinates of LED devices.

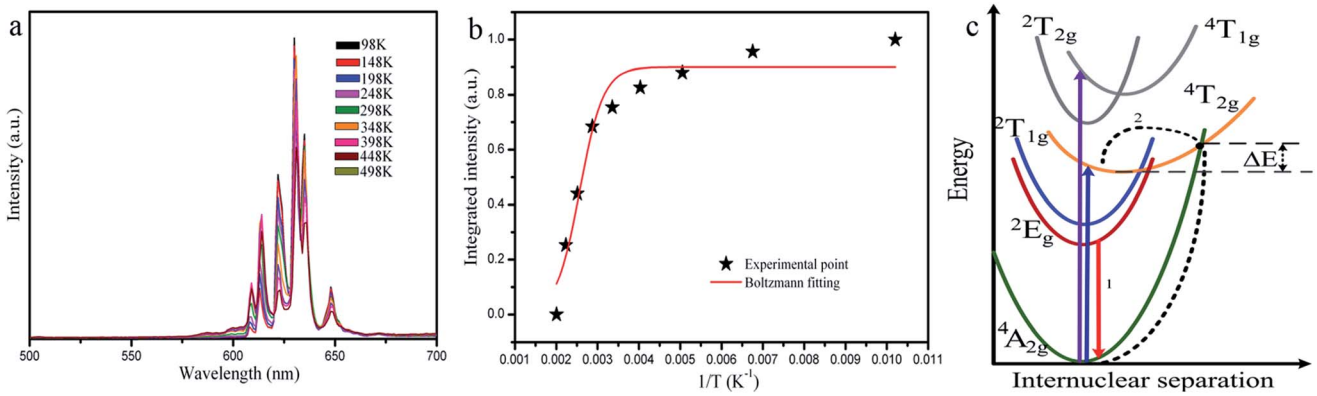

Fig. 9 (a) Emission spectra of $K_2NaAlF_6:Mn^{4+}$ upon excitation of 460 nm, (b) temperature dependence of the relative intensity of $^2E_g \rightarrow {}^4A_{2g}$ transition of Mn^{4+} in K_2NaAlF_6, and (c) configurational coordinate diagram for illustration the possible thermal quenching process of Mn^{4+} in the K_2NaAlF_6 host.

Table 1 Measured photometric and chromaticity for the LEDs

Sample	CIE coordinates (x, y)	CCT	R_a	Luminous efficiency
A	0.1460, 0.0359			24.52 lm W^{-1}
D	0.3530, 0.3956	4882 K	70.9	108.23 lm W^{-1}
E	0.3759, 0.4075	4310 K	78.7	60.22 lm W^{-1}

$K_2NaAlF_6:Mn^{4+}$ under 20 mA current excitation. The emission peak of blue light chip is ~460 nm, and it overlaps with the excitation spectrum of red phosphor $K_2NaAlF_6:Mn^{4+}$. Compared with the LED prepared by combining with YAG:Ce^{3+}, the prepared LEDs that blends YAG:Ce^{3+} and $K_2NaAlF_6:Mn^{4+}$ shows a warm white light property by the naked eye. The CIE chromaticity diagram and the object photograph of the LEDsdevices are exhibited in Fig. 10(b). The related photoelectric parameters such as correlated color temperature (CCT), color rendering index (CRI) and luminous efficacy of these LEDs, are listed in Table 1. The corresponding CIE coordinates of LEDs shift from cool white light (0.3530, 0.3956) to warm white light (0.3759, 0.4075). The CCT of the WLEDs is dropped from 4882 K to 4310 K, and the CRI improves from 70.9 to 78.7. However, the luminous efficiency of the LEDs decreases from 108.23 lm W^{-1} to 60.22 lm W^{-1}. These results indicate that the red phosphors can enhance LED performance and have potential applications in the field of indoor lighting.

4 Conclusions

In summary, a class of red phosphor $K_2NaAlF_6:Mn^{4+}$ was prepared by hydrothermal method, and its crystal structure, morphology, composition, optical properties were characterized. Under excitation of blue light, $K_2NaAlF_6:Mn^{4+}$ can give a red emission located at 633 nm ascribed to the transition of $^2E_g \rightarrow {}^4A_{2g}$. The influence of synthesis conditions, including the ratio of reaction materials, reaction temperatures and times, the concentrations of Mn^{4+} ions, on the crystal structure and optical properties of the $K_2NaAlF_6:Mn^{4+}$ had been discussed carefully. Moreover, the critical distance between adjacent Mn^{4+} in the K_2NaAlF_6 host was calculated. The concentration quenching phenomenon appearing in the $K_2NaAlF_6:Mn^{4+}$ is attributed to dipole–dipole interaction. The temperature dependent emission intensity shows that $K_2NaAlF_6:Mn^{4+}$ has excellent thermal stability and is suitable for the working temperature of LEDs. Furthermore, the warm white LED is fabricated by coupling the 460 nm blue chip with a mixture of yellow (YAG:Ce^{3+}) and red ($K_2NaAlF_6:Mn^{4+}$) phosphor, which has lower color temperature (4310 K), higher color rendering index (R_a = 78.7) and luminous efficacy of 60.22 lm W^{-1}. Therefore, $K_2NaAlF_6:Mn^{4+}$ is a promising red phosphor for warm white LEDs.

Conflicts of interest

There are no conflicts to declare.

Acknowledgements

This work was financially supported by the National Natural Science Foundation of P. R. China (NSFC) (Grant No. 51072026, 51573023) and the Development of science and technology plan projects of Jilin province (Grant No. 20170101185JC).

Notes and references

1 Y. Wang, T. Wen, L. Tang, L. Yang, W. Yang and Y. Zhao, *Dalton Trans.*, 2015, **44**, 7578–7585.
2 M. J. Lee, Y. H. Song, Y. L. Song, G. S. Han, H. S. Jung and D. H. Yoon, *Mater. Lett.*, 2015, **141**, 27–30.
3 L. Lv, X. Jiang, S. Huang, X. A. Chen and Y. Pan, *J. Mater. Chem. C*, 2014, **2**, 3879–3884.
4 S. Zhang, Y. Hu, H. Duan, Y. Fu and M. He, *J. Alloys Compd.*, 2017, **693**, 315–325.
5 Z. Wang, Y. Zhou, Y. Liu, Q. Zhou, L. Luo, H. Tan, Q. Zhang, G. Chen and J. Peng, *RSC Adv.*, 2015, **5**, 82409–82414.
6 X. Gao, Y. Song, G. Liu, X. Dong, J. Wang and W. Yu, *Dalton Trans.*, 2016, **45**, 17886–17895.
7 R. Cao, J. Huang, X. Ceng, Z. Luo, W. Ruan and Q. Hu, *Ceram. Int.*, 2016, **42**, 13296–13300.
8 H. Tan, M. Rong, Y. Zhou, Z. Yang, Z. Wang, Q. Zhang, Q. Wang and Q. Zhou, *Dalton Trans.*, 2016, **45**, 9654–9660.
9 T. T. Deng, E. H. Song, J. Sun, L. Y. Wang, Y. Deng, S. Ye, J. Wang and Q. Y. Zhang, *J. Mater. Chem. C*, 2017, **5**, 2910–2918.
10 E. Song, J. Wang, J. Shi, T. Deng, S. Ye, M. Peng, J. Wang, L. Wondraczek and Q. Zhang, *ACS Appl. Mater. Interfaces*, 2017, **9**, 8805–8812.
11 X. Ding, Q. Wang and Y. Wang, *Phys. Chem. Chem. Phys.*, 2016, **18**, 8088–8097.
12 S. Zhang, Y. Hu, H. Duan, L. Chen, Y. Fu, G. Ju, T. Wang and M. He, *RSC Adv.*, 2015, **5**, 90499–90507.
13 X. Jiang, Y. Pan, S. Huang, X. A. Chen, J. Wang and G. Liu, *J. Mater. Chem. C*, 2014, **2**, 2301–2306.
14 Y. Jin, Y. Hu, H. Wu, H. Duan, L. Chen, Y. Fu, G. Ju, Z. Mu and M. He, *Chem. Eng. J.*, 2016, **288**, 596–607.
15 S. P. Singh, M. Kim, W. B. Park, J.-W. Lee and K.-S. Sohn, *Inorg. Chem.*, 2016, **55**, 10310–10319.
16 J. Long, Y. Wang, R. Ma, C. Ma, X. Yuan, Z. Wen, M. Du and Y. Cao, *Inorg. Chem.*, 2017, **56**, 3269–3275.
17 X. Jiang, Z. Chen, S. Huang, J. Wang and Y. Pan, *Dalton Trans.*, 2014, **43**, 9414–9418.
18 R. Cao, X. Ceng, J. Huang, H. Ao, G. Zheng, X. Yu and X. Zhang, *Opt. Mater.*, 2016, **62**, 706–710.
19 X. Ding, G. Zhu, W. Geng, Q. Wang and Y. Wang, *Inorg. Chem.*, 2016, **55**, 154–162.
20 X. Q. Li, X. Su, P. Liu, J. Liu, Z. Yao, J. Chen, H. Yao, X. Yu and M. Zhan, *CrystEngComm*, 2015, **17**, 930–936.
21 H. Chen, H. Lin, Q. Huang, F. Huang, J. Xu, B. Wang, Z. Lin, J. Zhou and Y. Wang, *J. Mater. Chem. C*, 2016, **4**, 2374–2381.
22 H. Zhu, C. C. Lin, W. Luo, S. Shu, Z. Liu, Y. Liu, J. Kong, E. Ma, Y. Cao, R.-S. Liu and X. Chen, *Nat. Commun.*, 2014, **5**, 4312.

23 Y. Jin, Y. Fu, Y. Hu, L. Chen, H. Wu, G. Ju, M. He and T. Wang, *Powder Technol.*, 2016, **292**, 74–79.
24 Y. Jin, M.-H. Fang, M. Grinberg, S. Mahlik, T. Lesniewski, M. G. Brik, G.-Y. Luo, J. G. Lin and R.-S. Liu, *ACS Appl. Mater. Interfaces*, 2016, **8**, 11194–11203.
25 L.-L. Wei, C.-C. Lin, M. H. Fang, M. G. Brik, S.-F. Hu, H. Jiao and R.-S. Liu, *J. Mater. Chem. C*, 2015, **3**, 1655–1660.
26 Q. Shao, L. Wang, L. Song, Y. Dong, C. Liang, J. He and J. Jiang, *J. Alloys Compd.*, 2017, **695**, 221–226.
27 B. Wang, H. Lin, F. Huang, J. Xu, H. Chen, Z. Lin and Y. Wang, *Chem. Mater.*, 2016, **28**, 3515–3524.
28 C. Yang, Z. Zhang, G. Hu, R. Cao, X. Liang and W. Xiang, *J. Alloys Compd.*, 2017, **694**, 1201–1208.
29 Q. Zhou, Y. Zhou, Y. Liu, L. Luo, Z. Wang, J. Peng, J. Yan and M. Wu, *J. Mater. Chem. C*, 2015, **3**, 3055–3059.
30 H.-D. Nguyen, C. C. Lin, M.-H. Fang and R.-S. Liu, *J. Mater. Chem. C*, 2014, **2**, 10268–10272.
31 Y. Zhu, J. Yu, Y. Liu, M. G. Brik, L. Huang, T. Xuan and J. Wang, *RSC Adv.*, 2017, **7**, 30588–30593.
32 L. Huang, Y. Zhu, X. Zhang, R. Zou, F. Pan, J. Wang and M. Wu, *Chem. Mater.*, 2016, **28**, 1495–1502.
33 E. H. Song, J. Q. Wang, S. Ye, X. F. Jiang, M. Y. Peng and Q. Y. Zhang, *J. Mater. Chem. C*, 2016, **4**, 2480–2487.
34 H. Bode, H. Jenssen and F. Bandte, *Angew. Chem.*, 1953, **65**, 304.
35 T.-C. Lang, T. Han, L.-L. Peng and M.-J. Tu, *Mater. Chem. Front.*, 2017, **1**, 928–932.
36 Y. Zhu, L. Huang, R. Zou, J. Zhang, J. Yu, M. Wu, J. Wang and Q. Su, *J. Mater. Chem. C*, 2016, **4**, 5690–5695.
37 G. Blasse and G. J. Dirksen, *J. Solid State Chem.*, 1986, **65**, 283–286.
38 X. Gao, Y. Song, G. Liu, X. Dong, J. Wang and W. Yu, *CrystEngComm*, 2016, **18**, 5842–5851.
39 S.-S. Liang, M.-M. Shang, H.-Z. Lian, K. Li, Y. Zhang and J. Lin, *J. Mater. Chem. C*, 2017, **5**, 2927–2935.